

Gold Nanoparticle-Based Colorimetric Assay for the Direct Detection of Cancerous Cells

Colin D. Medley, Joshua E. Smith, Zhiwen Tang, Yanrong Wu, Suwussa Bamrungsap, and Weihong Tan*

Center for Research at the Bio/Nano Interface, Department of Chemistry and Shands Cancer Center, UF Genetics Institute and McKnight Brain Institute, University of Florida, Gainesville, Florida 32611

Early and accurate detection of cancer often requires time-consuming techniques and expensive instrumentation. To address these limitations, we developed a colorimetric assay for the direct detection of diseased cells. The assay uses aptamer-conjugated gold nanoparticles to combine the selectivity and affinity of aptamers and the spectroscopic advantages of gold nanoparticles to allow for the sensitive detection of cancer cells. Samples with the target cells present exhibited a distinct color change while nontarget samples did not elicit any change in color. The assay also showed excellent sensitivity with both the naked eye and based on absorbance measurements. In addition, the assay was able to differentiate between different types of target and control cells based on the aptamer used in the assay indicating the wide applicability of the assay for diseased cell detection. On the basis of these qualities, aptamer-conjugated gold nanoparticles could become a powerful tool for point of care diagnostics.

The key to the effective and ultimately successful treatment of diseases such as cancer is an early and accurate diagnosis. An early diagnosis is only possible with a sensitive method for the detection of the disease. Current methods are time-consuming, expensive, and require advanced instrumentation. A more cost-effective method requiring simple or no instrumentation yet still providing great sensitivity and accuracy would be ideal for point of care diagnosis. To accomplish this, we have developed the first colorimetric assay for the direct detection of cancer cells by using aptamer-conjugated gold nanoparticles (ACGNPs).

Aptamers are oligonucleotide strands that bind to their targets with high affinity and selectivity, which rival antibodies in their diagnostic potential.¹ Aptamers are able to fold into unique three-dimensional conformations that allow them to bind to selected molecules ranging in size from small organic molecules to proteins.^{2–5} As such, they have successfully been demonstrated

for protein detection and targeted therapeutic applications.^{6–10} In this work, the aptamers were selected using the cell-SELEX¹¹ methodology in which live whole cells served as the target instead of merely a single molecule. The cell-SELEX methodology also employs a negative selection step in which a negative cell line is used to remove any sequences that bind nonselectively to both cell types. This allows for multiple aptamers to be selected based solely on the unique surface properties of the target cells without any prior knowledge of the proteins or receptors on the cell surface. Therefore, the selectivity of the aptamers can be tuned based on how closely related the two cell types are in relation to each other to allow the selection of aptamers that can distinguish between different diseases or even different strains of the disease. Once selected the aptamers can be chemically synthesized allowing for different functional groups or labeling molecules to be easily integrated. This property combined with their selectivity and affinity makes them ideal for use in diagnostic assays or targeted therapy applications.

To make the assay colorimetric in nature, gold nanoparticles were utilized for their biofunctionalization, biostability, and spectral properties. Due to the plasmon resonance of gold nanoparticles, they possess strong distance-dependent optical properties. Once the gold nanoparticles come into proximity with one another their absorption spectra shift and their scattering profile changes resulting in a change in color and in the resulting absorption spectra of the sample.^{12–16} As a result of these properties, many techniques have been developed based on the aggregation of gold

* To whom correspondence should be addressed. Telephone: 352-846-2410. Fax: 352-846-2410. E-mail: tan@chem.ufl.edu.

- (1) Brody, E. N.; Gold, L. *Rev. Mol. Biotechnol.* **2000**, *74*, 5–13.
- (2) Ellington, A. D.; Szostak, J. W. *Nature* **1990**, *346*, 818–822.
- (3) Fang, X.; Cao, Z.; Beck, T.; Tan, W. *Anal. Chem.* **2001**, *73* (23), 5752–5757.
- (4) Famulok, M.; Mayer, G. *Curr. Top. Microbiol. Immunol.* **1999**, *243*, 123–136.
- (5) Li, J.; Fang, X.; Tan, W. *Biochem. Biophys. Res. Commun.* **2002**, *292*, 31–40.

- (6) Osborne, S. E.; Matsumura, I.; Ellington, A. D. *Curr. Opin. Chem. Biol.* **1997**, *1*, 5–9.
- (7) Yang, C. J.; Jockusch, S.; Vicens, M.; Turro, T.; Tan, W. *Proc. Natl. Acad. Sci. U.S.A.* **2005**, *102*, 17278–17283.
- (8) Nutiu, R.; Li, Y. *Angew. Chem., Intl. Ed.* **2005**, *44*, 1061–1065.
- (9) Farokhzad, O. C.; Jon, S.; Khademhosseini, A.; Tran, T. T.; LaVan, D. A.; Langer, R. *Cancer Res.* **2004**, *64*, 7668–7672.
- (10) Liu, J.; Lu, Y. *J. Am. Chem. Soc.* **2007**, *129*, 8634–8643.
- (11) Shangguan, D.; Li, Y.; Tang, Z.; Cao, Z. C.; Chen, H. W.; Mallikaratchy, P.; Sefah, K.; Yang, C. J.; Tan, W. *Proc. Natl. Acad. Sci. U.S.A.* **2006**, *103*, 11838–11843.
- (12) Sandrock, M. L.; Foss, C. A., Jr. *J. Phys. Chem. B* **1999**, *103*, 11398–11406.
- (13) Storhoff, J. J.; Lazarides, A. A.; Mucic, R. C.; Mirkin, C. A.; Letsinger, R. L.; Schatz, G. C. *J. Am. Chem. Soc.* **2000**, *122*, 4640–4650.
- (14) Grant, C. D.; Schwartzberg, A. M.; Norman, T. J., Jr.; Zhang, J. Z. *J. Am. Chem. Soc.* **2003**, *125*, 549–553.
- (15) Storhoff, J. J.; Elghanian, R.; Mucic, R. C.; Mirkin, C. A.; Letsinger, R. L. *J. Am. Chem. Soc.* **1998**, *120* (9), 1959–1964.
- (16) Reynolds, R. A., III; Mirkin, C. A.; Letsinger, R. L. *J. Am. Chem. Soc.* **2000**, *122* (15), 3795–3796.

nanoparticles to detect ions, genes, and proteins.^{17–23} The surface enhancement effect of gold nanoparticles has also been utilized for surface enhanced Raman scattering detection and study of cells^{24–26} while the strong near-IR absorbance of the aggregated gold nanoparticles has also been used for imaging and hyper-thermal therapy of cancer cells.^{27,28} However, instead of simple aggregation of the gold nanoparticles using genes or proteins, the ACGNPs are targeted to assemble on the surface of a specific type of cancer cell through the recognition of the aptamer to its target on the cell membrane surface as shown in the schematic in Figure 1A. The assembly of the ACGNPs around the cell surface causes a shift in the absorption spectra of the particles as the gold nanoparticles are in enough proximity for their surface plasmon resonances to overlap. As the gold nanoparticles now behave as a larger gold structure, the light scattering and absorption properties of the gold nanoparticles are altered as well, resulting in the majority of the signal transduction in the assay. In the sample, the individual gold nanoparticles interact inefficiently with light due to the size of the particle in relationship to the wavelength of the light. Once the gold nanoparticles assemble around the cell, the surface plasmon interaction results in the gold nanoparticles acting like a larger gold structure. The larger micrometer-scaled structure can very efficiently interact with the light and exhibits significantly increased scattering and absorption coefficients compared to the individual nanoparticles.

Through taking advantage of the unique properties of the aptamers and gold nanoparticles, we have developed an assay that is colorimetric in nature and has excellent selectivity between target and control cells. Being able to distinguish cancerous from noncancerous samples quickly and without any costly or complex instrumentation would be a very powerful tool for point of care diagnostics and even allow for the large-scale screening of particular diseases prior to more costly and invasive procedures.

EXPERIMENTAL SECTION

Aptamer Synthesis. An ABI3400 DNA/RNA synthesizer (Applied Biosystems, Foster City, CA) was used for the synthesis of all aptamer sequences. A ProStar high-pressure liquid chromatograph (HPLC; Varian, Walnut Creek, CA) with a C18 column (Econosil, 5 μ , 250 \times 4.6 mm) from Alltech (Deerfield, IL) was

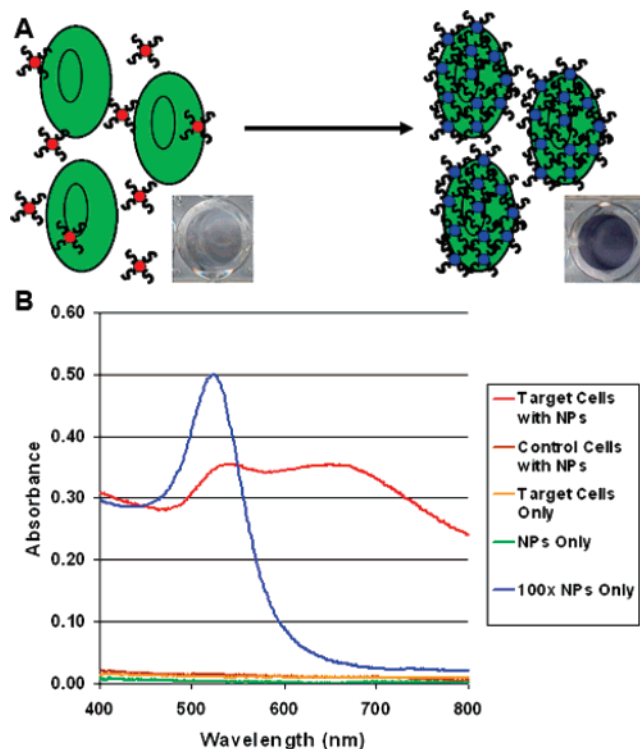


Figure 1. (A) Schematic representation of the ACGNP based colorimetric assay. (B) Plots depicting the absorption spectra obtained for various samples analyzed using ACGNPs. The spectra illustrate the differences in spectral characteristics observed after the ACGNPs bind to the target cells.

used to purify all fabricated DNA. A Cary Bio-300 UV spectrometer (Varian) was used to measure absorbances to quantify the manufactured sequences. All oligonucleotides were synthesized by solid-state phosphoramidite chemistry at a 1- μ mol scale. The completed sequences were then deprotected in concentrated ammonia hydroxide at 65 $^{\circ}$ C overnight and further purified twice with reversed-phase HPLC on a C-18 column. The CEM and Ramos aptamers were synthesized with the following sequences, respectively; 5'-TTT AAA ATA CCA GCT TAT TCA ATT AGT CAC ACT TAG AGT TCT AGC TGC TGC GCC GCC GGG AAA ATA CTG TAC GGA TAG ATA GTA AGT GCA ATC T-3'; 5'-AAC ACC GGG AGG ATA GTT CGG TGG CTG TTC AGG GTC TCC TCC CGG TG-3'. The thiol group was added on column using a 3'-thiol modifier CPG (Glen Research, Sterling, VA) to the 3' position.

ACGNPs Synthesis. In a 2-mL microcentrifuge tube, 1 mL of the 20-nm gold colloid nanoparticles (GNPs), containing 7.0×10^{11} particles/mL, taken directly from the manufacturer (Ted Pella, Inc., Redding, CA) was centrifuged for 15 min at 14 000 rpm. The GNPs were washed three times with 1-mL aliquots of 5 mM phosphate buffer (PB) pH 7.5 by decanting the supernatant, adding fresh PB, dispersing by sonication, and centrifuging for 15 min at 14 000 rpm. From decantation to dispersion, the wash step was performed within 3–5 min. After the final wash step, the GNPs were dispersed in 1 mL of the PB. To each washed GNP sample, 150 μ L of a 10 μ M thiol-labeled DNA sequence was incubated for 3–5 days at 4 $^{\circ}$ C. The samples were sonicated to disperse the GNPs every 12 h. When the incubations were completed, the samples were centrifuged at 14 000 rpm for 5 min and the samples washed as described previously with the PB. After

- (17) Thanh, N. T. K.; Rosenzweig, Z. *Anal. Chem.* **2002**, *74*, 1624–1628.
 (18) Elghanian, R.; Strohoff, J. J.; Mucic, R. C.; Letsinger, R. L.; Mirkin, C. A. *Science* **1997**, *277*, 1078–1081.
 (19) Park, S.-J.; Lazarides, A. A.; Mirkin, C. A.; Letsinger, R. L. *Angew. Chem., Int. Ed.* **2001**, *40*, 2909–2912.
 (20) Norsten, T. B.; Frankamp, B. L.; Rotello, V. M. *Nano Lett.* **2002**, *2*, 1345–1348.
 (21) Huang, C. C.; Huang, Y. F.; Cao, Z.; Tan, W.; Chang, H. T. *Anal. Chem.* **2005**, *77* (17), 5735–5741.
 (22) Zhao, W.; Chiuman, W.; Brook, M. A.; Li, Y. *ChemBioChem.* **2007**, *8*, 7, 727–731.
 (23) Xu, X.; Han, M. S.; Mirkin, C. A. *Angew. Chem., Int. Ed.* **2007**, *46*, 3468–3470. Lee, J. S.; Han, M. S.; Mirkin, C. A. *Angew. Chem., Int. Ed.* **2007**, *46*, 4093–4096.
 (24) Tang, H. W.; Yang, X. B.; Kirkham, J.; Smith, D. A. *Anal. Chem.* **2007**, *79* (10), 3646–3653.
 (25) Lee, S.; Kim, S.; Choo, J.; Shin, S. Y.; Lee, Y. H.; Choi, H. Y.; Ha, S.; Kang, K.; Oh, C. H. *Anal. Chem.* **2007**, *79* (3), 916–922.
 (26) Huang, X.; El-Sayed, I. H.; Wei, Q.; El-Sayed, M. A. *Nano Lett.* **2007**, *7* (6), 1591–1597.
 (27) Loo, C.; Lowery, A.; Halas, N.; West, J.; Drezek, R. *Nano Lett.* **2005**, *5* (4), 709–711.
 (28) El-Sayed, I. H.; Huang, X.; El-Sayed, M. A. *Cancer Lett.* **2006**, *239* (1), 129–135.

the final wash, each GNP sample was dispersed in 0.25 mL of PB with $\sim 6.0 \times 10^{11}$ particles, and the samples stored at 4 °C until used.

Cells. CCRF-CEM cells (CCL-119 T-cell, human acute lymphoblastic leukemia) and Ramos cells (CRL-1596, B-cell, human Burkitt's lymphoma) were obtained from American Type Culture Association. The cells were cultured in RPMI medium supplemented with 10% fetal bovine serum (FBS) and 100 IU/mL penicillin–streptomycin. The cell density was determined using a hemocytometer prior to any experiments. After which, ~ 1 million cells dispersed in RPMI cell media buffer were centrifuged at 920 rpm for 5 min, redispersed in dye-free cell media three times, and then redispersed in 5 mL of dye-free cell media. The actual cell numbers were then extrapolated based on the cell density. During all experiments, the cells were kept in an ice bath at 4 °C to prevent internalization of any of the materials. Unless specified, the cell amount used in the experiments is $\sim 25\,000$ cells.

Assay Protocol. For each assay, 1.0×10^{10} ACGNPs were utilized in a total volume of 300 μ L unless specified otherwise in the text. The cells and ACGNPs were mixed, then incubated for 30 min at 4 °C in a 500- μ L microcentrifuge tube, and then transferred to a BD Falcon 96-well transparent microplate (Fisher Scientific, Pittsburgh, PA). After incubation, the assays in the microplates were imaged with an Epson Stylus CX3200 flatbed scanner and the spectra were measured in a Tecan Safire Microplate reader (Mannedorf, Switzerland). The absorbance was measured in the microplate scanning from 400 nm to 900 nm at a 1 nm resolution. The nanoparticle absorbance was subtracted out from each measurement. All data analysis was performed using Microsoft Excel. TEM images were taken with a JEOL TEM 2010F transmission electron microscope on a copper grid.

RESULTS AND DISCUSSION

To demonstrate the principle behind the assay, it was first determined whether the ACGNPs could differentiate between target cells and control cells. For these experiments, CCRF-CEM acute leukemia cells were used as target cells while Ramos, a Burkitt's lymphoma cell line, were used as control cells. An aptamer sequence with high selectivity and affinity to the CCRF-CEM cells was conjugated to 20-nm gold nanoparticles through a thiol functional group on the aptamer sequence. The five samples are as follows: 1.0×10^{10} ACGNPs, 1.0×10^{10} ACGNPs with 10 000 target cells, 1.0×10^{10} ACGNPs with 10 000 control cells, 10 000 target cells with no ACGNPs, and 1.0×10^{12} ACGNPs in cell media. The absorption spectrum for each sample is shown in Figure 1B. The results establish that the absorbance of the ACGNPs with 10 000 target cells is significantly higher than the same amount of ACGNPs with 10 000 control cells, the same amount of target cells without ACGNPs, or with only the ACGNPs. These results indicate that the ACGNPs are binding selectively to the target cells and that the assembly of the ACGNPs around the target cells causes an increase in the absorption and scattering of the solution. The excellent selectivity of the assay stems from the highly selective aptamer utilized in the experiment and also from the nature of the gold nanoparticles themselves. While in some forms of analysis, the nonspecific binding of a small amount of nanoparticles could cause the generation of a false positive signal, the gold nanoparticles rely on the large-scale assembly of the particles to change their spectral properties. Therefore, the

nonspecific association of a small amount of gold nanoparticles would be insufficient to generate any signal transduction causing the assay to be even more selective. The signals from the nonbinding samples were too low to determine whether there was a shift in the spectra accompanying the binding of the ACGNPs to the target cells. To determine whether a shift occurred, a spectrum from a sample of ACGNPs that was 100 times more concentrated was also measured and plotted in Figure 1B (100 \times NPs only). This spectrum indicates that a red shift in the absorption occurs when the ACGNPs bind to the target cells. The large increase in the measured absorbance of the samples stems from the ability of the assembly of nanoparticles to absorb and scatter light efficiently. The individual 20-nm ACGNPs do not scatter or absorb light as efficiently as the nanoparticles assembled around the 15- μ m cells. This results in an overall increase in the measured absorbance of the sample in addition to the observed shift in the spectrum.

To verify that the nanoparticles were assembling on the surface of the target cells, TEM images of the target and control cells mixed with the ACGNPs were taken. For these images, the assay protocol was observed for both target and control cells followed by deposition onto a copper grid for TEM imaging. The samples were then allowed to dry before TEM imaging. The results for the target and control cells are shown in Figure 2. Based on the TEM images, the gold nanoparticles appear to be assembling on the surface of the target cells. However, with the control cells, the TEM images indicate that the ACGNPs do not assemble on the control cells. This indicates that the aptamers on the ACGNPs do cause the assembly of the ACGNPs on the cell surface leading to the spectral changes that have been previously described.

The next experiment was conducted to optimize the gold nanoparticle size to be used in the assay. The two primary criteria for the optimization were to identify the greatest signal difference between the target and control cells and the greatest red shift of the particle spectra. The greatest signal change between target and control cells would identify the most sensitive assay in terms of detection capability while the greatest red shift would allow the most sensitive detection respective to samples of bodily fluids that typically have maximum absorbances below 600 nm. For this experiment, four different particles sizes were tested: 5, 20, 50, and 100 nm. The amount of nanoparticles for each size was 1.0×10^{10} ACGNPs except for the 5-nm nanoparticles in which 1.0×10^{11} nanoparticles were used to compensate for the low signal intensity observed for these particles. Figure 3A shows the spectrum for each size of nanoparticle with target cells. Based on the spectra, the 50-nm gold nanoparticles have the greatest measurable red shift and absorbance past 600 nm. The 5-nm nanoparticles showed very little red shift, indicating the nanoparticles may not be getting to within enough proximity to each other for their surface plasmons to interact. This is further supported by the lack of any color change associated with the addition of target cells and no net increase in the magnitude of the absorbance. The 100-nm gold nanoparticle exhibited only a single peak with a shift less than 50-nm nanoparticles although this could be due to the limitations of the instrument, which is designed for UV–vis measurements while any second peak for the 100-nm nanoparticles could extend farther into the near-IR. This could be due to the increased repulsive forces of 100-nm nanoparticles

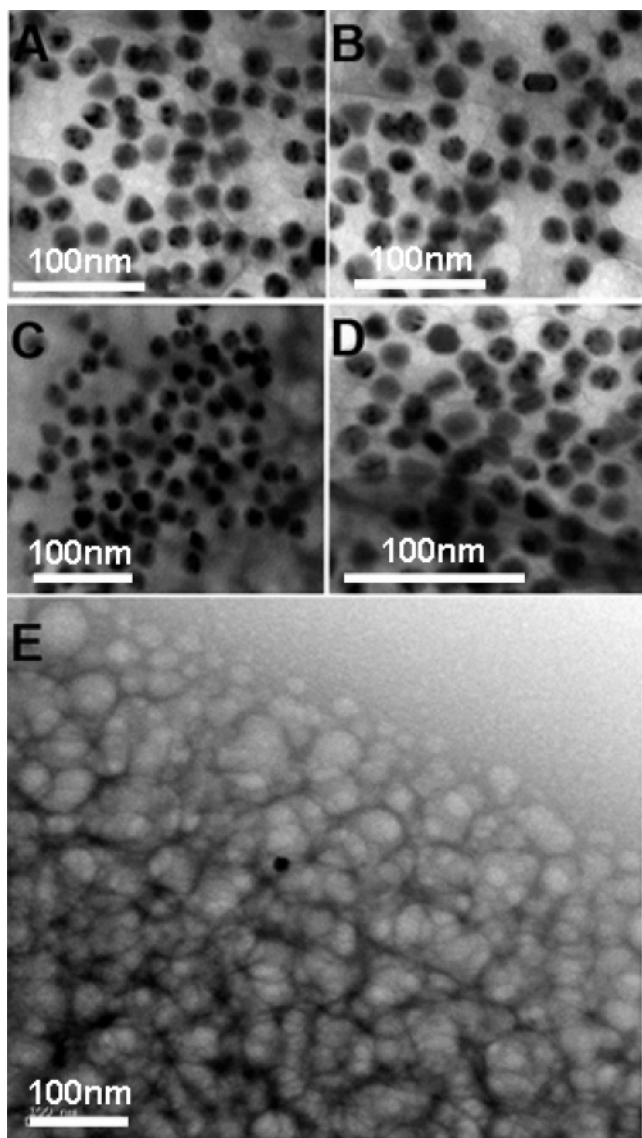


Figure 2. (A–D) TEM images of ACGNPs assembled on different regions of the target cell surface. (E) Image of the control cell surface showing no assembly of the ACGNPs although nonspecific binding does occur. Scale bars for each image are shown in white.

preventing a large amount of nanoparticles from assembling on the surface; however, this would not explain the increase in the intensity of the absorbance signal from the nanoparticles. The 20-nm nanoparticles also had a significant red shift. The 20-, 50-, and 100-nm particles also exhibited a distinct color change when target cells were present (data not shown) while no noticeable difference was observed with the 5-nm nanoparticles. When comparing the signal enhancements of the different particle sizes, the signal from the assay's response to target cells was divided by the signal from the control cells to determine the enhancement using the absorbance maximum for each nanoparticle. The enhancement for each particle size is plotted in Figure 3B. Based on the enhancements, the 20-nm particles exhibited the greatest signal change and still possessed a significant red shift in the absorbance. Based on these qualities, the 20-nm nanoparticles were used in all subsequent experiments although in future work more significant optimization for each particle size will be completed to more thoroughly evaluate the particles.

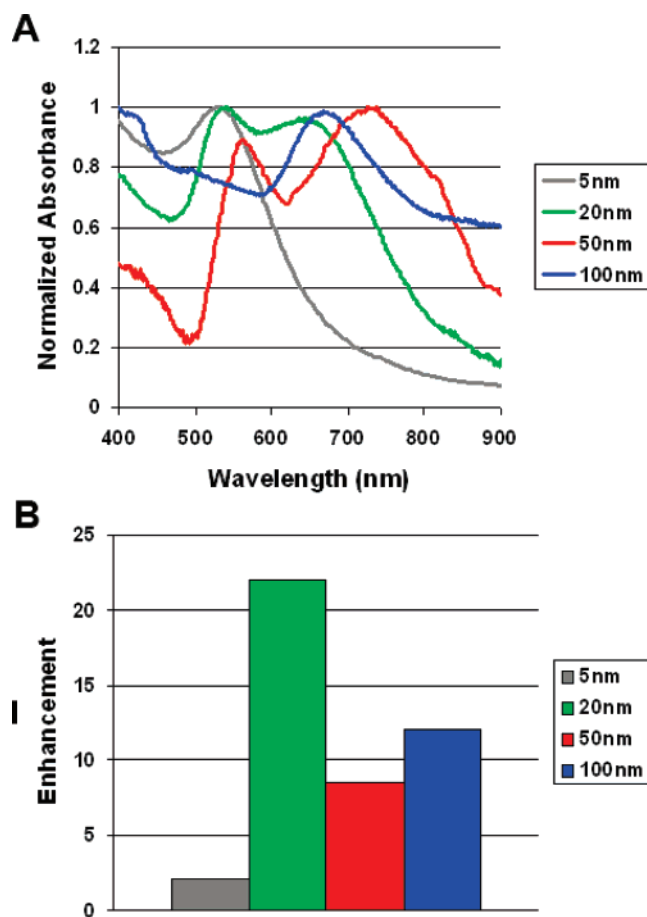


Figure 3. (A) Spectra of different sizes of the ACGNPs with target cells to evaluate the red shift based on particle size. (B) The enhancement of the ACGNPs that is a measure of the signal difference between the assay's response to target cells versus the same amount of control cells.

With the initial concept and development of the assay demonstrated, the next step was to verify that the assay is indeed colorimetric and could differentiate between different amounts of cells based on color. In order to accomplish this, 1.0×10^{10} ACGNPs were incubated with increasing amounts of target cells. This was repeated with the same amounts of control cells for comparison. The image of both cell types is shown in Figure 4A. The results clearly show that the samples with more target cells have a darker color until finally little difference is seen after 20 000 with the naked eye. In the control cells, the samples remain almost colorless and there is no significant difference between the samples regardless of the amount of cells present. Thus, the assay allows for the detection of target cells with the naked eye. The assay also proved to be quite sensitive as 1000 cells could be readily detected by the naked eye. The amount of nanoparticles used was carefully selected to allow saturation of the highest number of cells while using the lowest amount of nanoparticles to reduce the background coloration of the solution, thus facilitating an easier detection of the lower end of the cell concentration.

In order for a more sensitive detection than allowed by the human eye, the samples were also analyzed using a microplate reader. The spectra for the different amounts of control and target cells are shown in Figure 4B and C, respectively. The absorption spectra correlate well with the colorimetric results in that the

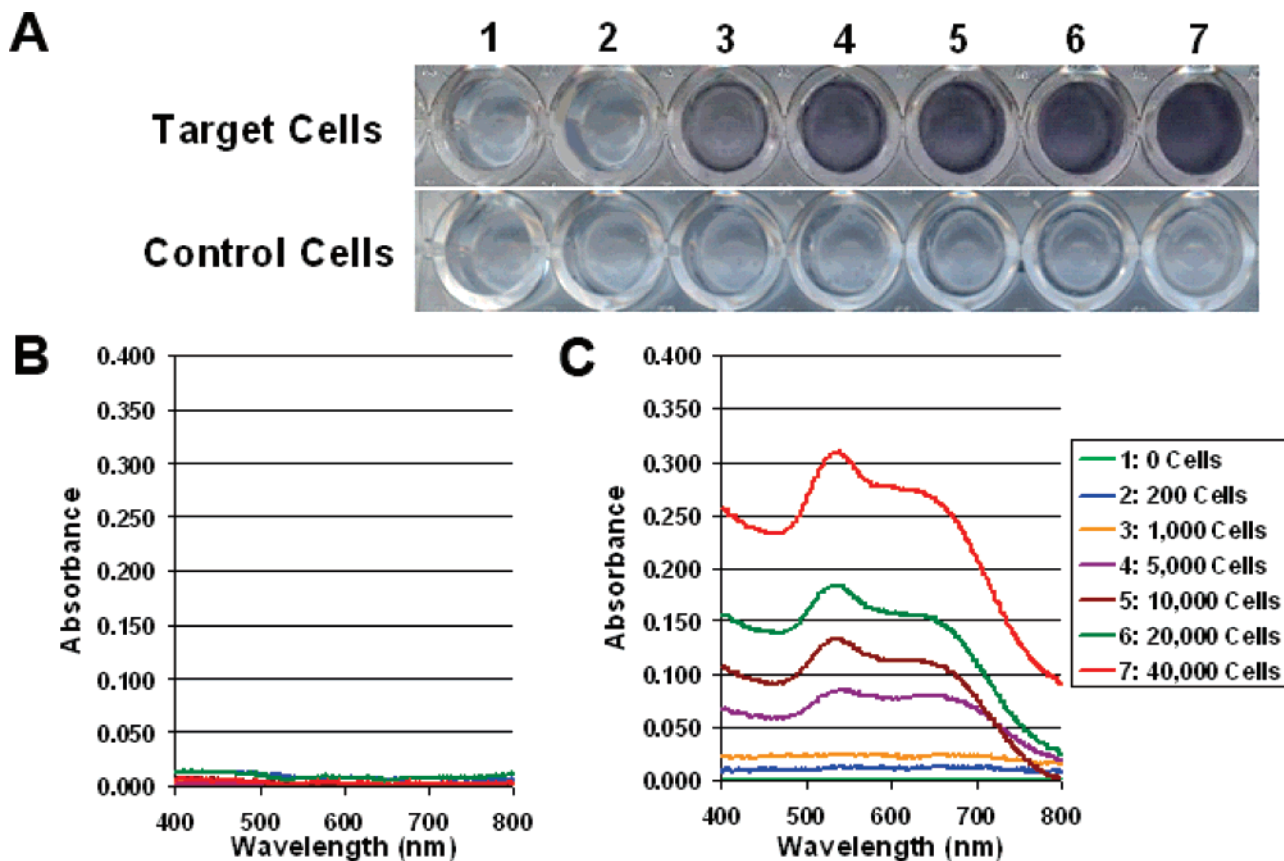


Figure 4. (A) Images of ACGNPs with increasing amounts of target (top) and control cells (bottom). The amount of cells used in each sample is given in the legend on the bottom right. (B) Absorption spectra of the control cell samples with ACGNPs in Figure 2A. (C) Absorption spectra of the target samples with ACGNPs in Figure 2A.

samples with an increasing amount of target cells absorb light more intensely. There is little change in the ACGNP absorption spectra of the control cell samples regardless of the amount of cells present. This is most likely a consequence of the selectivity of the aptamer itself and also the nature of the gold nanoparticles. Realistically, absolute selectivity is difficult to achieve regardless of the molecular recognition element employed, and it is highly likely that a few of the ACGNPs bind nonselectively to the control cells. However, in order to generate a signal from ACGNPs, there needs to be many gold nanoparticles in proximity; therefore, even if there is a limited amount of nonselective binding occurs, it is very unlikely it will be to the extent to cause a positive response to the assay further increasing the apparent selectivity of the assay to the target cells. It is also interesting to note that the peak shape of the spectra changes with the amount of target cells as the absorbance maximums undergo a small blue shift and the peak at roughly 530 nm increases relative to the red-shifted peak at roughly 650 nm. This is mostly likely due to the saturation of the nanoparticles at higher cell concentrations resulting in the gold nanoparticles being spaced further apart and incomplete coverage of the cells. It is likely that this trend will continue with even higher concentrations of the cells leading to the eventual decrease in sensitivity. However, that amount of cells far exceeds the amount of cancer cells that would be in an actual clinical sample with cancers like lymphomas and leukemias likely possessing cell numbers under 10 000 cells and other exfoliated epithelial-based cancer cells numbering far fewer yet so the oversaturation of the ACGNPs is not believed to be a major concern.

In order to determine the limit of detection for the assay, the previous experiment was repeated four more times. The absorbance at 650 nm was then recorded for each amount of cells and plotted in Figure 5A. The assay showed an excellent dynamic range with standard deviations ranging from 6 to 10%. Based on three times the standard deviation of the blank measurement, the limit of detection of the target cells was calculated to be 90 cells. In addition, this experiment was repeated with control cells to measure their response to the assay. The ACGNPs had no response to the control cells at the lower cell concentrations as these samples had signals comparable to the blank. At the higher cell concentrations, the ACGNPs had a small response to the control cells although it was still significantly lower than even the smallest concentration of target cells that were evaluated. Based on these results, the assay for direct cell detection has demonstrated excellent sensitivity and selectivity.

In order to truly evaluate the assay, more complicated samples also needed to be analyzed to determine whether the assay could be useful for actual samples. In order to accomplish this, the assay was also used on several samples of FBS. In these samples, the 50 000 cells were spiked into FBS and then the 1.0×10^{10} ACGNPs were added. Target and control cells were spiked into different samples and then after incubation with the ACGNPs their spectra were measured using the microplate reader. The absorbance at 650 nm from the three samples was averaged and plotted in Figure 5B; for comparison, the signals of the same amount of cells in cell media were also measured. The target cells in FBS clearly show a significantly higher signal than the control cells in the

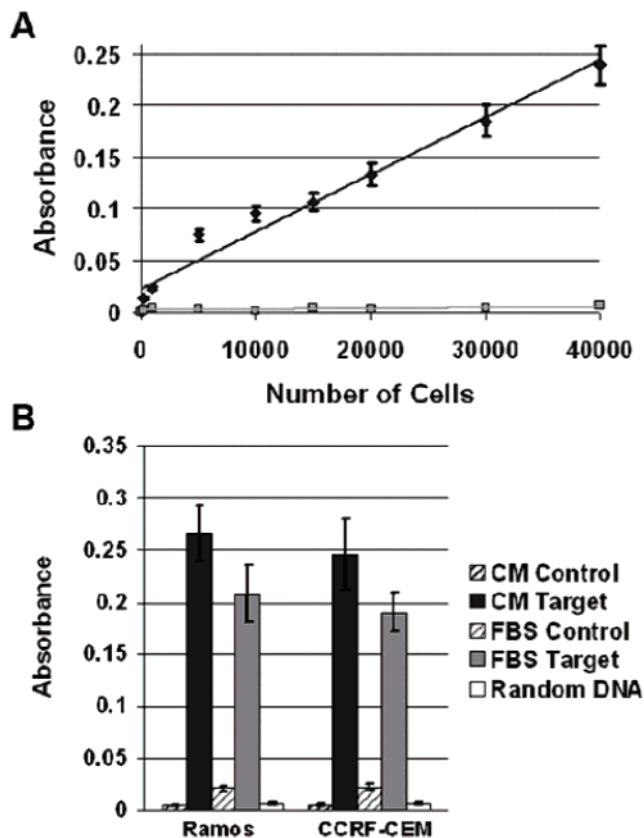


Figure 5. (A) Calibration curve illustrating the relationship between the amount of cells and the absorbance intensity at 650 nm for both target cells (black) and control cells (gray). The assay shows a very good dynamic range in addition to excellent sensitivity. (B) Bar graph showing the change in intensity between the target cells and control cells at 650 nm in both cell media (CM) and fetal bovine serum (FBS) for both cell types. The graph also shows the response of a nontargeting aptamer sequence to each cell type (random DNA).

FBS, indicating that the assay functions as expected in even complex environments. Colorimetric determination, however, proved difficult due to the color of the FBS. In future experiments with more complex samples, further sample preparation to remove any colored species may be necessary for any colorimetric detection. Regardless, spectroscopic detection of the target cells in FBS was achieved without any further sample preparation steps. In an effort to show the assay is applicable to other cell types, this experiment was repeated along with the same experiment in cell media using an aptamer that is selective for the Ramos cell line while using the CCRF-CEM cells as a negative control. Again, the ACGNPs showed excellent sensitivity and selectivity to the target cells regardless of the line of cells targeted in both the cell media and in the FBS. As an additional control, 50 000 cells of each type were also incubated with 1.0×10^{10} ACGNPs with a nontarget aptamer sequence. The results are shown in Figure 5B (random DNA). The sequence had no specificity for either cell

type and produced no noticeable change in either the color of the solution or the absorbance of the sample versus controls. This indicates that the ACGNPs must be able to bind to the surface of the cells in order to produce a change in their spectral properties.

CONCLUSION AND DISCUSSION

ACGNPs have been demonstrated for the sensitive and selective detection of cancer cells through utilizing the unique spectral properties of gold nanoparticles and the excellent selectivity of aptamers. The assay is the first colorimetric assay for the direct detection of cancerous cells. In addition, spectroscopic detection using ACGNPs proved successful for even complex samples like FBS and demonstrated excellent sensitivity and selectivity. Little nonselective binding was observed, most likely due to the characteristics of the gold nanoparticles in that any binding of a few nanoparticles to the control cells would not have been enough to drastically alter that spectral property of the particles. We have proven that ACGNPs can be assembled on a cell membrane surface for spectral change, providing a direct visualization of cancer cells.

In addition, the assay was demonstrated on two different cell types that had cell-SELEX aptamers selected for them. This indicates that the similar colorimetric assay could be developed for any cell types where aptamers can be generated based on the cell surface differences between cell types. This could include colorimetric assay for different varieties of cancers or even infectious diseases. Currently, cell-SELEX aptamers have been generated for several types of leukemia and lymphoma as well as small cell lung cancer and liver cancer, suggesting that the development of colorimetric assays for the detection of these diseases is possible.

Future work will include the further development of the assay including optimizing the particle size, incubation times, and sample preparation methods for complex samples. After optimization, the assay will be tested on more complex samples including blood samples using both colorimetric and spectroscopic detection. This assay has the potential to provide a rapid, high-throughput, sensitive, and cost-effective approach for the early and accurate detection of cancer through the utilization of aptamers and nanotechnology.

ACKNOWLEDGMENT

The authors thank Dr. Kim Sapsford for her technical expertise and useful comments, and the support of NIH grants 2 R01 GM066137 and R21CA122648, and ONR grant N00014-07-1-0982. We also acknowledge a State of Florida Center of Excellence grant on Bio/nano sensors.

Received for review September 30, 2007. Accepted November 12, 2007.

AC702037Y